Fuel Processing Technology 272 (2025) 108208

Contents lists available at ScienceDirect

Fuel Processing Technology

journal homepage: www.elsevier.com/locate/fuproc

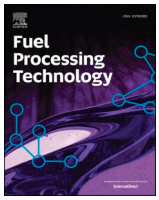

Research article

Performance improvement and emissions reduction of methanol fuelled marine dual-fuel engine with variable compression ratio

Panagiotis Karvounis *, Gerasimos Theotokatos

Maritime Safety Research Centre, Department of Naval Architecture, Ocean, and Marine Engineering, University of Strathclyde, Glasgow G4 0LZ, United Kingdom

ARTICLE INFO

Keywords:
Marine dual fuel engines
Variable compression ratio
Methanol
NOx emissions
Shipping sustainability
Decarbonisation

ABSTRACT

Methanol use in marine engines is associated with challenges pertaining to misfiring and knocking. This study aims at parametrically optimising a marine dual-fuel four stroke engine considering variable compression ratio (VCR) settings and methanol direct injection with 90 % energy fraction. CFD models are developed and validated against experimental data. Parametric runs are employed in 20, 55 and 90 % load, with compression ratio ranging 11–19, to reveal the optimal CR values for each load considering the engine performance and emissions parameters along with constraints on combustion efficiency and stability. The sustainability index is employed to assess the environmental sustainability of the engine under optimal VCR settings compared to FCR. The results reveal that the engine thermal efficiency for CR 19, 16 and 12 at low, medium and high loads respectively increases by 7 %, 2 % at low and medium loads, whereas, decreases by 4 % at the high load. The engine with the proposed VCR settings achieves the compliance with the IMO Tier III limits and increases its sustainability index by 21 % compared to the fixed compression ratio. This study provides insights for the effective use of high methanol energy fractions in marine dual engines, thus contributing to the shipping sector sustainability.

1. Introduction

The shipping sector seeks to effectively address its decarbonisation, pledging for net-zero CO_2 emissions per transport work by 2050 [1]. Methanol is perceived as a short-term solution in the shipping sector transition towards zero-carbon fuels [2] especially when it is produced by using renewable energy from agricultural resins [3]. Moreover, pertinent technoeconomic analyses proved that use of methanol fuel as a decarbonisation solution or large ship fleets is financially plausible [4].

Methanol use reduces carbon dioxide emissions due to the lower carbon to hydrogen ratio (compared to diesel), whereas its high auto-ignition temperature requires the injection of high reactivity pilot fuel to initiate combustion. Reviewing 55 studies dealing with methanol use in compression ignition engines concluded that a clear trade-off between thermal efficiency and methanol energy fraction cannot be established [5]. The two main methanol combustion methods in compression ignition engines are the diffusive and premixed combustion associated with the in-cylinder direct and port injection, respectively [6]. Both methods have benefits and drawbacks. Premixed injection facilitates more homogeneous methanol-air mixtures leading to faster combustion with lower NOx emissions [7]. However, the significant probability of knocking at medium and high loads, constraints the diesel energy substitution rate to 40–60 % [8–11]. Conversely, direct methanol injection can facilitate methanol energy fractions up to 95 % [12] with benefits on thermal efficiency and hydrocarbon emissions [13].

Due to its high enthalpy of evaporation, methanol reduces the in-cylinder reactivity leading to reduced maximum in-cylinder temperature and pressure [14]. This may cause misfiring at low and medium loads with high diesel substitution rates [15]. On the contrary, at high loads, the increased laminar flame speed leads to extensive knocking due to the high in-cylinder reactivity [16]. To mitigate methanol quenching effect, considerable in-cylinder reactivity is achieved by increasing the charging air temperature, which results in higher NOx emissions [17], or by increasing the compression ratio, which may result in unstable combustion at other loads. To reduce the knocking propensity, exhaust gas recirculation is deemed essential [18], resulting in the engine thermal efficiency penalisation.

To facilitate the decarbonisation of the shipping sector and enhance its sustainability, it is essential to use high shares of green methanol as a fuel in marine engines. Split injection strategies that include two or more methanol injection stages (an early injection during the compression stroke and following injections closer to or after the top dead centre) can

* Corresponding author.
E-mail address: panagiotis.karvounis@strath.ac.uk (P. Karvounis).

https://doi.org/10.1016/j.fuproc.2025.108208
Received 6 February 2025; Received in revised form 4 March 2025; Accepted 12 March 2025
Available online 19 March 2025

mitigate misfiring in low loads [39]. While these strategies are promising in low loads, they result to significant knocking in high loads, the mitigation of which requires excessively large split ratios for methanol injection [40]. These contradictory split injection requirements in the complete engine operating envelope introduce challenges for their consistent application. Advancing the pilot fuel injection timing can mitigate knocking in medium and high loads for a dual-fuel engine with 94 % methanol energy fraction [41], it is limited, however, by misfiring in low loads (due to the reduced in-cylinder reactivity) [42]. Christensen et al. [43] demonstrated the multi-fuel capability of engines with variable compression ratio (VCR) setting in various loads.

Integrating Variable Compression Ratio (VCR) technology into large-bore engines, presents significant challenges pertinent to the structural integrity of components. VCR system for large-bore engines highlighted that while VCR can improve fuel efficiency by approximately 5.5 %, the design must address increased mechanical complexity and ensure durability under varying compression ratios [45].

The preceding literature review advocates that most studies deal with fixed compression ratio, lacking investigations of VCR technologies in marine dual-fuel engines operating with high methanol energy fractions. Although methanol has potential to decarbonise the maritime industry, challenges such as misfiring at low loads and knocking at high loads remain unaddressed. Moreover, studies focusing on the VCR use in marine large-bore engines to address these challenges and meet international emission regulations such as IMO Tier III are not reported.

Hence, this study aims at parametrically optimising a marine dual-fuel four stroke engine considering VCR settings and methanol direct injection with 90 % energy fraction. The novelty of this study stems from: (i) the investigation of variable compression ratio settings for the considered engine operating with high methanol energy fractions; (ii) the identification of optimal settings to achieve improved engine performance and reduced emissions, and; (iii) the use of sustainability index for the appraisal of the engine environmental impact.

2. Methodology

The methodology followed in the study consists of eight steps. Step 1 focuses on the incorporation of the characteristics and settings of the considered marine engine. Step 2 focuses on the development of the CFD model for the diesel operation of the marine engine, using the CONVERGE software. The model considers in-cylinder diesel direct injection, whereas the injection parameters are derived from the engine shop tests report. Step 3 deals with the grid sensitivity study where the grid is selected compromising accuracy and computational effort. The validation of the CFD model against experimental data is performed in Step 4. Step 5 focuses on the development of CFD models for the dual-fuel operation with methanol considering as baseline the validated CFD model. The latter considers 90 % methanol energy fraction (MEF) and direct injection of both fuels from different nozzles of the same injector. Step 6 focuses on defining the operating envelope for the investigated engine with VCR, and identification of ranges for stable combustion. Step 7 includes the cases description for the fixed and variable compression ratio settings. Step 8 employs the derived results to comparatively assess the engine operation with fixed and variable compression ratio settings. The impact of VCR on the indicated thermal efficiency, combustion efficiency, NOx emissions and decarbonisation targets are identified and discussed, providing insights for the operation of marine dual fuel engines with high methanol fractions. The developed CFD model considers ideal gas state for the thermodynamic behaviour of the in-cylinder working medium; diesel and methanol are injected considering trapezoidal injection pulse [29]; and the power output per cylinder is deemed same for all the engine cylinders.

2.1. CFD model, grid sensitivity and experimental validation

The developed CFD models employ the cylinder geometric characteristics of the considered marine engine. To reduce the computational effort, and considering the cylinder and injector symmetries, a sector is selected corresponding to one sixth of the engine cylinder. The initial conditions for the dual-fuel operation of the considered marine engine are presented in Table A1 (Appendix) and are determined employing steady-state thermodynamic modelling and literature data. The sub-models for the droplet breakup are KH-RT [20] and for the collisions is NTC [21]. The extended Zeldovich model [22] is used for the NOx estimation, which is calibrated to match shop test NO data. Turbulence is calculated via the RANS k-ε model, whereas the reaction mechanism used in this study is the one proposed by Andrae & Head [24] that can effectively capture the reaction pathways of alcohol fuels (like methanol) and diesel. This mechanism is a semi detailed one consisting of 672 reactions and 143 species yielding best trade-off between accuracy of capturing in-cylinder behaviour and computational expense. The engine methanol energy fraction (MEF) is defined according to:

$$MEF = \frac{m_{CH_3OH}\, LHV_{CH_3OH}}{(m_D\, LHV_D) + \left(m_{CH_3OH}\, LHV_{CH_3OH}\right)} \quad (1)$$

where m is the mass of the fuels considered and LHV the lower heating value expressed in kJ/kg.

For the in-cylinder direct injection of both fuels, a single multi-hole injector with different nozzles for each fuel is considered (for more information regarding potential injectors advise [46,47]). Furthermore, keeping constant injection pressure ensures that the fundamental atomisation and spray formation characteristics remain consistent during diesel and methanol injection. Injecting the fuel at high pressure assures uniform atomisation and proper spray penetration, affecting the combustion efficiency. The injector tilt angle is set at 62.5° and spray cone angle at 17.5°, whereas the injection rate shape is trapezoidal as it is deemed beneficial for emissions [54]. A dual common rail system is considered, where each fuel has its own rail connected to the injector. The injection pressure for both fuels is assumed at 1000 bar. Since a common rail system is considered in most methanol/diesel dual-fuel engines, the injection pressure is the same. Separate piezoelectric actuators control the injection timings of each fuel separately. Methanol fuel is injected at 80 °CA BTDC whereas pilot diesel is injected at 12 °CA BTDC. Early injection of methanol during the compression stroke, leads to adequate mixing with charge air [15], reduction of compression work [25] and lower injection pressure requirements. VCR concept is realisable in marine engines by including mechanical adjustment of cylinder head or connecting rod thereby, altering the clearance volume and hence compression ratio. When operational switch from high to low compression ratio is required, bypass valve can be utilised to allow for pressure reduction in-cylinder.

The validation of the developed CFD model is conducted considering the in-cylinder pressure data acquired during shipboard measurements. Fig. 1(a)–(c) shows the predicted and measured in-cylinder pressure as well as the heat release rate for 30 %, 50 % and 90 % loads. The data are filtered and corrected as described in Tsitsilonis et al. [26] prior to calculating the heat release rate. For the diesel mode, the root mean square error was found to be less than 3 bar for all loads. Deviations from the measured values are attributed to the inherent uncertainty of the CFD sub models as well as engine degradation [27]. Furthermore, the simulated and experimental heat release profile is calculated using the first law of thermodynamics, however, small deviations pertain to the different assumptions and input for the heat transfer rate determination.

Due to the lack of experimental data with methanol for marine engines, the developed CFD model was further validated using reported data for a small-scale high-speed diesel engine operating in a dual fuel mode employing methanol port injection with 30 % MEF at 75 % load [30,33]. According to Fig. 1(d) results, the error for the maximum in-cylinder pressure calculated at 0.5 %, whereas the crank angle at the maximum pressure was simulated at 9.1 °CA ATDC instead of the measured 7.5 °CA ATDC. The CFD model overpredicts the first peak of

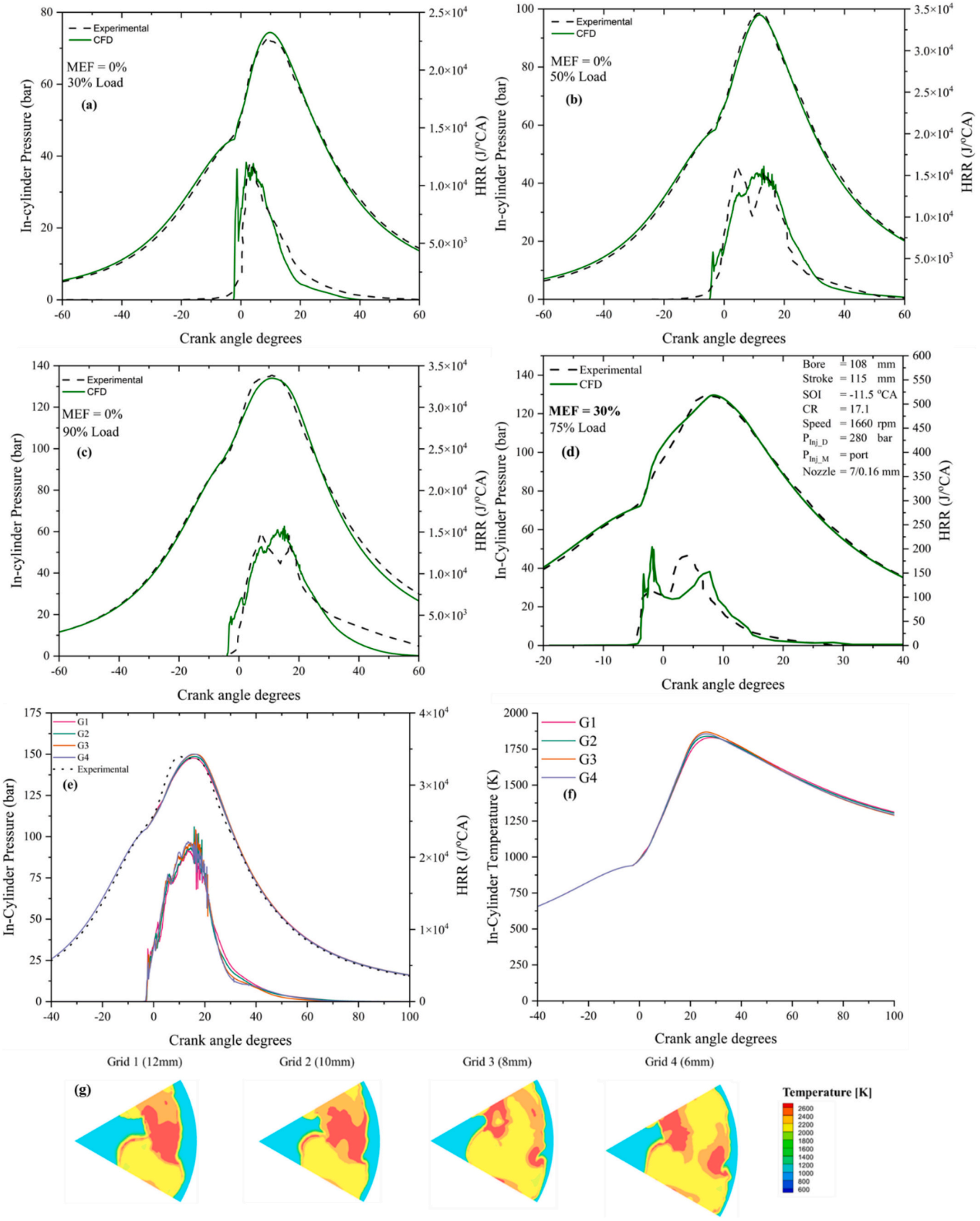

Fig. 1. CFD model validation results for diesel operation in: (a) 30 % load, (b) 50 % load, (c) 90 % load. (d) CFD model validation results for a light-duty diesel engine operating in 75 % load with 30 % MEF. Grid sensitivity study results for the four grids listed in Table A2 for (e) the in-cylinder pressure, and; (f) in-cylinder temperature. (g) Spatial distributions of the in-cylinder temperature for the four grids.

Table 1
Settings of the investigated cases for fixed and variable compression ratio.

Case	p_{IVC}[a] (bar)	T_{IVC} (K)	Methanol/Diesel SOI[b] (°CA BTDC)	Methanol/Diesel Injection Pressure (bar)	Methanol/Diesel Injection Duration (°CA)	Load (%)	EGR (mass %)	CR
FCR-a	1.74	380	80/12	1000	22/2	20	0	14
FCR-b	2.8	380			45/4	55	8	14
FCR-c	3.8	380			65/5	90	12	14
VCR-a	1.74	340			22/2	20	0	15 to 19
VCR-b	2.8	340			45/4	55	0	13 to 17
VCR-c	3.8	360			65/5	90	0	11 to 13

[a] IVC: inlet valve closing.
[b] SOI: start of injection.

heat release rate, corresponding to the premixed part of combustion and subsequently results in higher pressure from experimental between 5 and 0 °CA BTDC. The measured in-cylinder pressure data are used for the heat release rate calculation. Due to engine resonance, the heat release calculations require median-averaging smoothing. The empirical value of specific heat ratio for diesel operation is assumed for the dual-fuel mode calculations introducing inherent uncertainty due to different species in-cylinder. Furthermore, during the experiments, methanol injection in the intake port results in inhomogeneous air-fuel mixture. Conversely, the numerical model considers fully homogenous mixture and calculates the specific heat ratio for the dual-fuel operation at each crank angle step. Hence, this explains the slight differences in the benchmarked curves. The calculated root mean square error is 6 bar and which is around 4 % of the peak pressure yielding CFD behaviour within accepted errors [53]. The emissions validation is presented in appendix Fig. A1.

According to the retrieved results, the reaction mechanism, and the sub-models for spray, droplets, combustion, turbulence and heat transfer are considered validated. In international literature, models with similar root mean square variations are deemed validated as presented in the pertinent studies [50–52]. Hence, it is inferred that the developed CFD model can be employed with the highest possible confidence for the

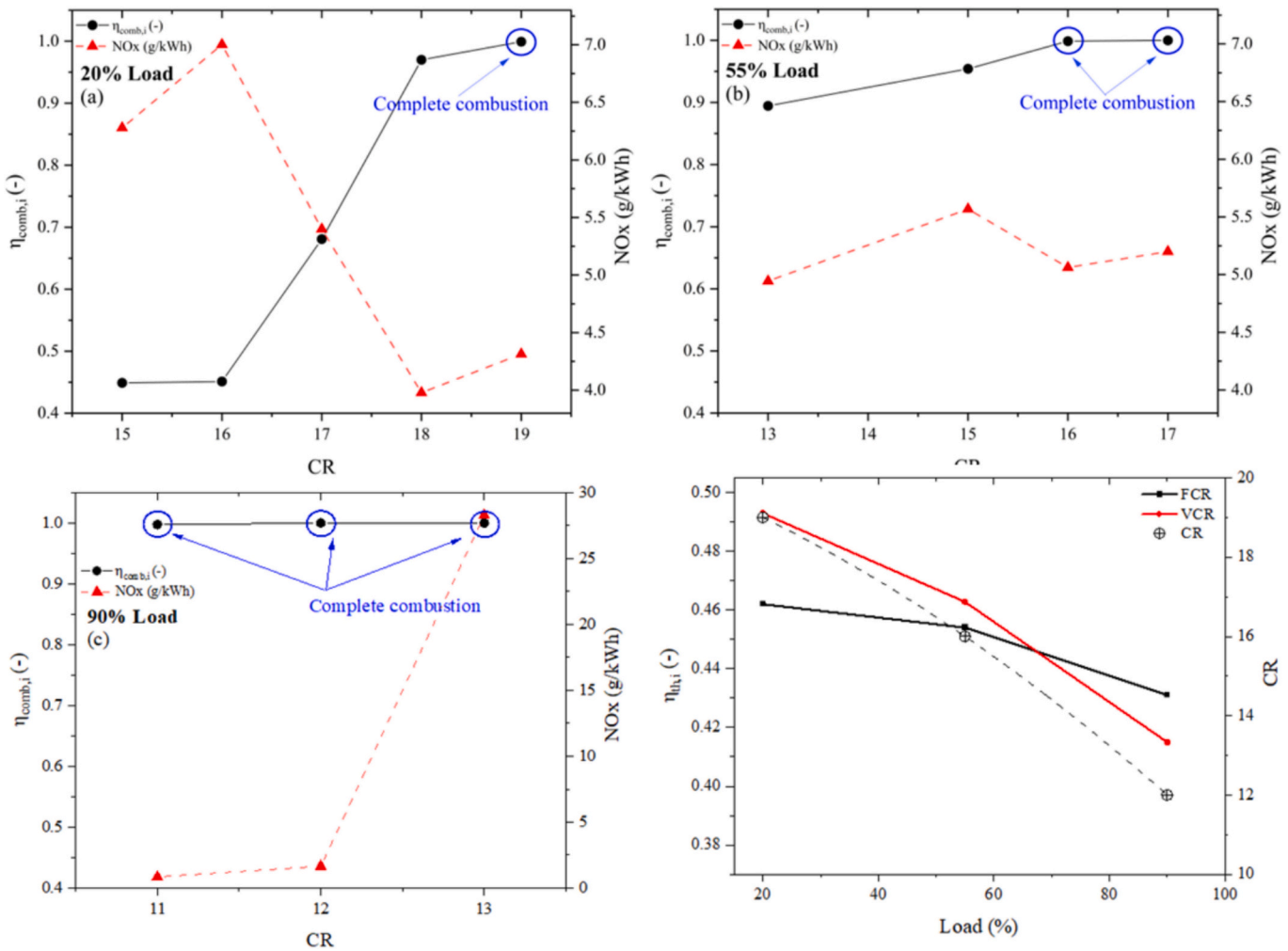

Fig. 2. (a–c) Combustion efficiency and NOx emissions versus CR for the three investigated loads; (d) thermal efficiency, NOx emissions and CR versus load for the engine with FCR and VCR settings derived from the parametric optimisation study (for VCR).

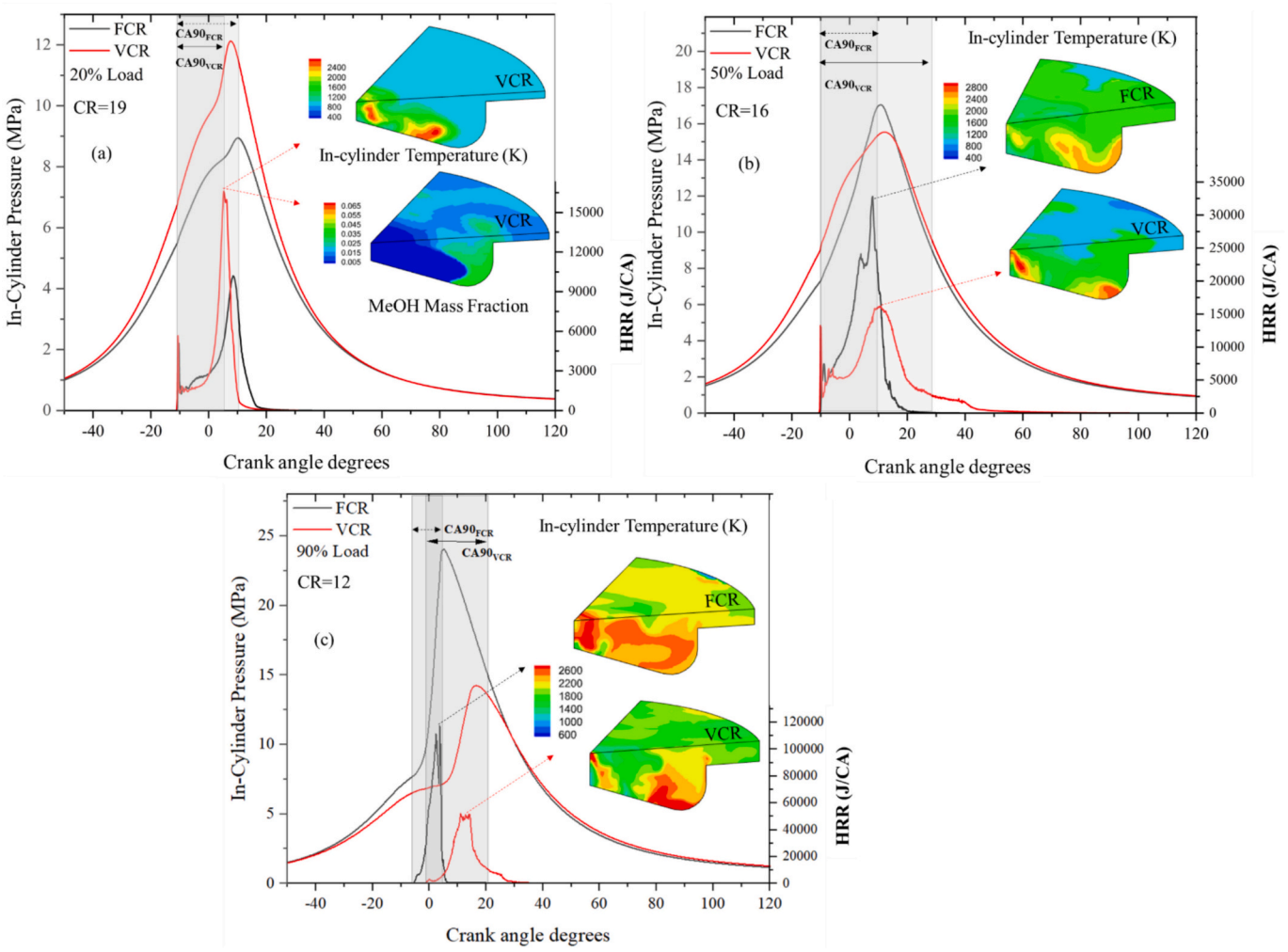

Fig. 3. In-cylinder pressure and heat release rate for (a) 20 % load, (b) 50 % load and (c) 90 % load fixed and variable compression ratio.

simulation of the considered variable and fixed compression ratio cases.

A grid sensitivity study is performed considering four different grids, the particulars of which are listed in Table A2 (Appendix). These grids contain cells of 12, 10, 8 and 6 mm coupled with adaptive mesh refinement between 80 °CA BTDC and 135 °CA ATDC. Fig. 1(e)–(f) present the in-cylinder pressure, heat release rate and temperature respectively for the four grids. Fig. 1(g) shows the spatial variation for the in-cylinder temperature for the considered grids. The results indicate that a base grid of 8 mm with level 4 velocity and temperature embedding exhibits the minimum error compared to the respective experimental values.

2.2. Cases description

The considered test cases along with the inputs regarding the temperature and pressure at the inlet valve closing, engine load, EGR and compression ratio (CR) are presented in Table 1. The considered cases include fixed and variable compression ratio settings, with the former to include EGR of 0 %, 8 % and 12 % at 20, 55 and 90 % loads respectively.

The baseline compression ratio of the engine is 14 and remains constant for the fixed compression ratio (FCR) cases. A parametric investigation is conducted for the variable compression ratio engine that includes the CR variation at each examined load. For 20 % load, CR varies between 15 and 19, for 55 % load between 13 and 17, whereas for 90 % load between 11 and 13. These CR values represent the operational limitations of engine designs with VCR [35].

The parametric optimisation considers thirteen cases corresponding to VCR settings, to define the CR values at each load that exhibits the best trade-off between indicated thermal efficiency and NOx emissions. The design of simulations is based on Latin Hyperqube sampling method to reduce computational effort [19]. EGR is not considered for the cases with VCR to avoid the thermal efficiency penalisation [23,34]. The settings for all the cases are selected to correspond to stable operation and close to complete combustion conditions. The temperature and pressure at the inlet valve closing (IVC) were determined through a parametric investigation [32] yielding that for the VCR cases lower temperature is required.

The VCR engine settings are realised by adjusting the piston position within the cylinder, thereby modifying the combustion chamber clearance volume. Recent industrial developments indicate that incorporating a piston with variable deck heights through a hydraulic control system allows to control the volume of the lubricating oil and hence vertically adjust the piston position [43,44]. A controlling system allows the regulation of oil amount based on the engine load providing continuous adjustment of the piston position.

Compliance with IMO limits for the E3 test cycle (propeller curve) entails the satisfaction of Eq. (2). The Tier-II and Tier-III limits for the investigated engine with nominal speed of 500 rev/m are 10.53 and 2.59 g/kWh, respectively [28].

$$\sum_{i=1}^{4} w_i \, BSNOx_i < BSNOx_{Tier\,j} \tag{2}$$

Table 2
Rate of pressure rise, CA50 and CA90 for the low, medium and high load operation of the VCR engine type.

Load	CR	Rate of Pressure Rise (MPa/°CA)	CA50 (°CA)	CA90 (°CA)
20 %	19	2.26	5.3	17.4
50 %	16	0.99	10.6	29.3
90 %	12	2.48	3.2	7.2

where i of 1 to 4 resembles to 25, 50, 75 and 100 % loads respectively; w_i represents the weight for each load (being 0.2, 0.5, 0.15 and 0.15 for 25, 50, 75 and 100 % loads respectively); and $BSNOx_i$ indicates the brake specific NOx emissions for each load.

To evaluate the Tier limits compliance, the following operating points (according to the E3 test cycle) were modelled for the FCR and VCR settings: (a) nominal (100 %) load and speed, (b) 75 % load and 91 % speed, (c) 50 % load and 80 % speed, and (d) 25 % load and 60 % speed.

To evaluate the sustainability performance of the engine with VCR compared to FCR, several indicators are estimated. Those include global warming (GWP), acidification (AP), aerosol formation (AFP) and eutrophication (EP) potentials. The employed equations are provided in the appendix. The sustainability index (SI) is estimated according to the following equation considering different weights for each indicator [36,37].

$$SI = w_{GWP}\frac{GWP_{FCR}}{GWP_{VCR^*}} + w_{AP}\frac{AP_{FCR}}{AP_{VCR^*}} + w_{AFP}\frac{AFP_{FCR}}{AFP_{VCR^*}} + w_{EP}\frac{EP_{FCR}}{EP_{VCR^*}} \quad (3)$$

where, w denotes the weight for each potential, being 0.5, 0.2, 0.1 and 0.2 for GWP, AP, AFP and EP, respectively.

3. Results

Fig. 2(a–c) presents the combustion efficiency and NOx emissions for the different compression ratios and loads for the VCR cases. In the low load, CR increases from 14 (baseline) to 19. Since the engine with VCR employs lower charging temperature, and due to the low cetane number of methanol fuel, combustion is inhibited. Consequently, incomplete combustion occurs for CR values of 15, 16 and 17. For CR 16 the in-cylinder temperature is increased yielding higher NOx emissions. Conversely, as CR increases NOx reduce due to faster combustion and hence lower temperature maxima reached in-cylinder. Combustion efficiency increases with CR duo to the higher in-cylinder reactivity. Complete combustion ($\eta_{comb} = 100$ %) at 20 % load is exhibited for CR of 19 as the in-cylinder reactivity increase, providing the required energy for the combustion reactions onset.

In the medium load (55 %) the dual-fuel engine still exhibits misfiring conditions as the ignition energy provided by pilot diesel is insufficient. However, increase of charging pressure and engine speed, offer more favourable in-cylinder conditions for methanol combustion. For this load, CR is variated between 13 and 17. Complete combustion is achieved for CRs 16 and 17 whereas NOx emissions are found to be 5 g/kWh and 5.5 g/kWh, respectively. As CR increases from 16 to 17, greater in-cylinder temperature is achieved yielding increased NOx emissions. In the high load (90 %), the effect of high laminar flame speed of methanol along with the increased in-cylinder reactivity, are responsible for rapid combustion that leads to extensive knocking. To suppress knocking, CR is reduced to 12. For all the examined cases, complete combustion is achieved ($\eta_{comb} > 99$ %). Further reduction of CR to 11 would push the engine towards the misfiring limits. As CR decreases, the in-cylinder temperature and pressure reduce, hence slowing the chemical reaction kinetics and resulting in a longer ignition delay. The diffusive combustion of low cetane fuels provides lower peak temperatures, leading to lower NOx emissions [35]. Considering the presented results, it is proposed for the engine with VCR to use CR of 19, 16 and 12 in the low, medium and high loads, respectively. For intermediate loads, a piece-wise linear change of CR is proposed as demonstrated in Fig. 2 (d).

Fig. 2(d) presents the indicated thermal efficiency for engine with VCR and FCR. The VRC settings were derived from the parametric optimisation study for each load. The indicated thermal efficiency increases by 7 %, 2 % in 20, 55 % loads whereas decreases by 4 % in 90 % load. For the fixed compression ratio cases, the indicated thermal efficiency drops from 46.4 % to 43.2 % as the load increase due to the EGR use. As load increases, rapid combustion occurs due to high laminar flame velocity of methanol. Therefore, the EGR use is essential to facilitate stable combustion conditions. However, the EGR reduces the in-cylinder reactivity prolonging combustion, and hence results in reduced indicated thermal efficiency.

For the low load, increasing compression ratio from 14 to 19, provides greater expansion ratio resulting in greater energy utilisation, yielding 7 % increase in the indicated thermal efficiency for the VCR settings compared to FCR. As compression ratio increases, better atomisation is achieved (due to higher air density resisting the

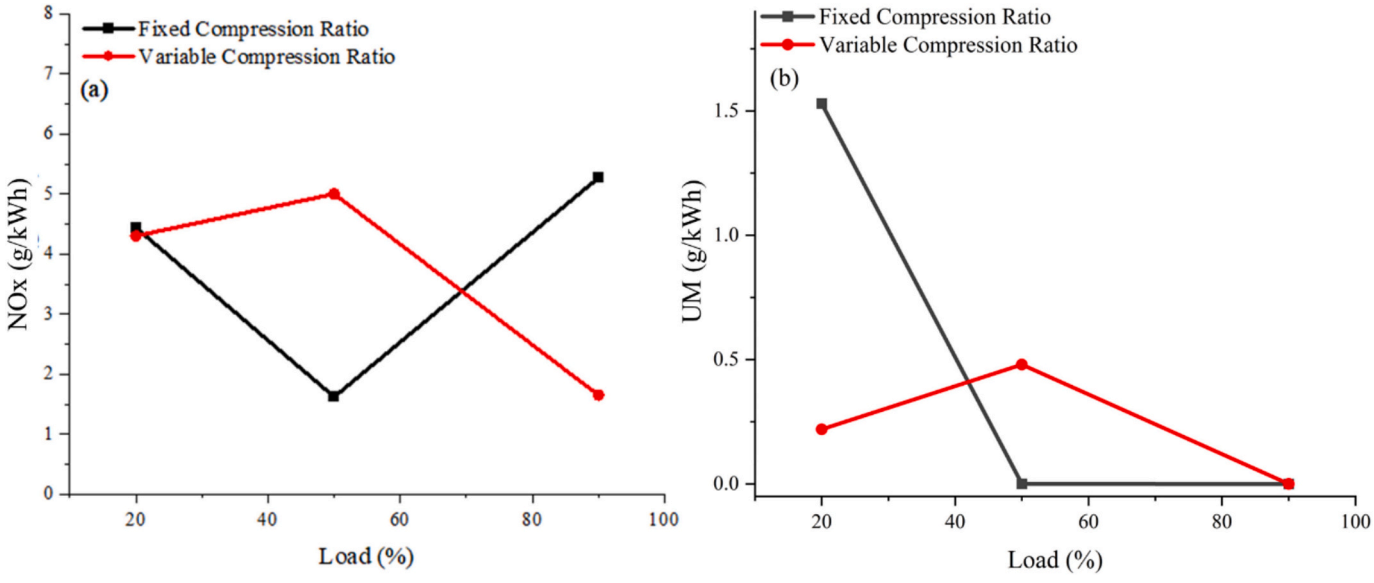

Fig. 4. (a) NOx and (b) UM emissions versus load for the FCR and VCR settings.

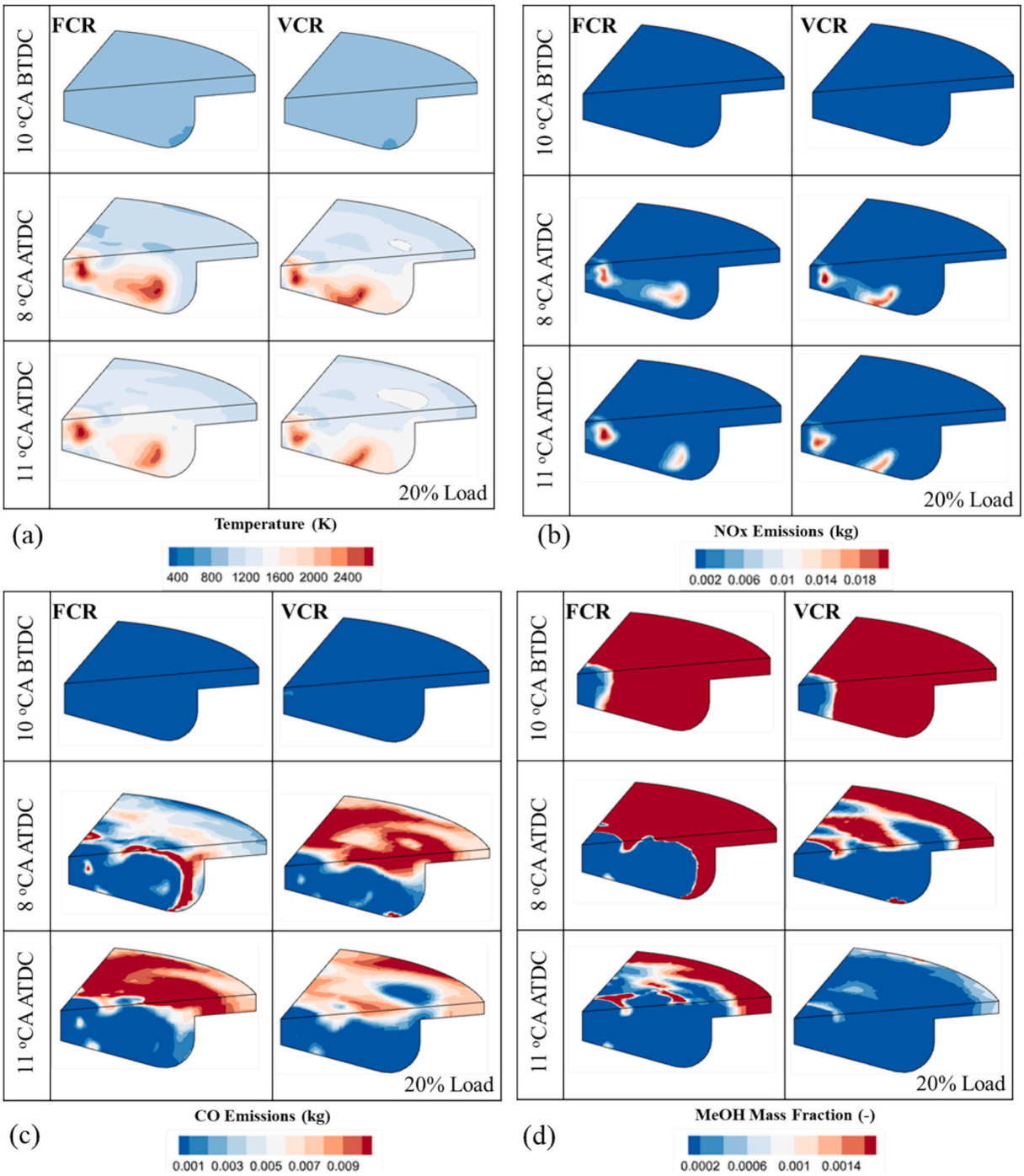

Fig. 5. Contours of (a) temperature, (b) NOx emissions, (c) CO emissions and (d) Methanol mass fraction spatial distribution in-cylinder for fixed and variable compression ratio engine types at 20 % load.

penetration of fuel spray, breaking it into smaller droplets, improving mixing efficiency [48]) promoting complete combustion conditions. The compression ratio increase at the medium load (55 %) from 14 to 16 leads to complete combustion conditions improving the indicated thermal efficiency to 46.3 %. At the high load (90 %) onset of knocking phenomena appear. For FCR settings, these are mitigated by considering EGR (12 % mass). However, for VCR settings, the CR value decrease to 12 reduces the in-cylinder reactivity resulting in stable combustion conditions. However, the indicated thermal efficiency reduces from 43.1 % to 41.5 % for VCR due to the low expansion ratio.

Fig. 3 illustrates the in-cylinder pressure and heat release rate for VCR and FCR in 20, 55 and 90 % loads. For the low load and VCR (higher CR value compared to FCR), the combustion occurs faster. CA90 is reached at 5 ^{o}CA ATDC for VCR compared to 11 ^{o}CA ATDC for FCR. Since injection of methanol has finished before the start of combustion, the heat release rate is characterised by a partially premixed combustion of methanol and diesel [38]. The first peak of the curve refers to the pilot diesel combustion. The second one at 5 ^{o}CA TDC is attributed to methanol combustion. As observed from the contours of Fig. 3a, methanol is concentrated in the bottom of the cylinder however the mixture is highly heterogenous. VCR and FCR experience similar trends however, the higher CR is responsible for higher peak in heat release rate for the VCR.

For the medium load, CR is increased from 14 to 16 and hence the compression side of the pressure curve is higher for the VRC case. The

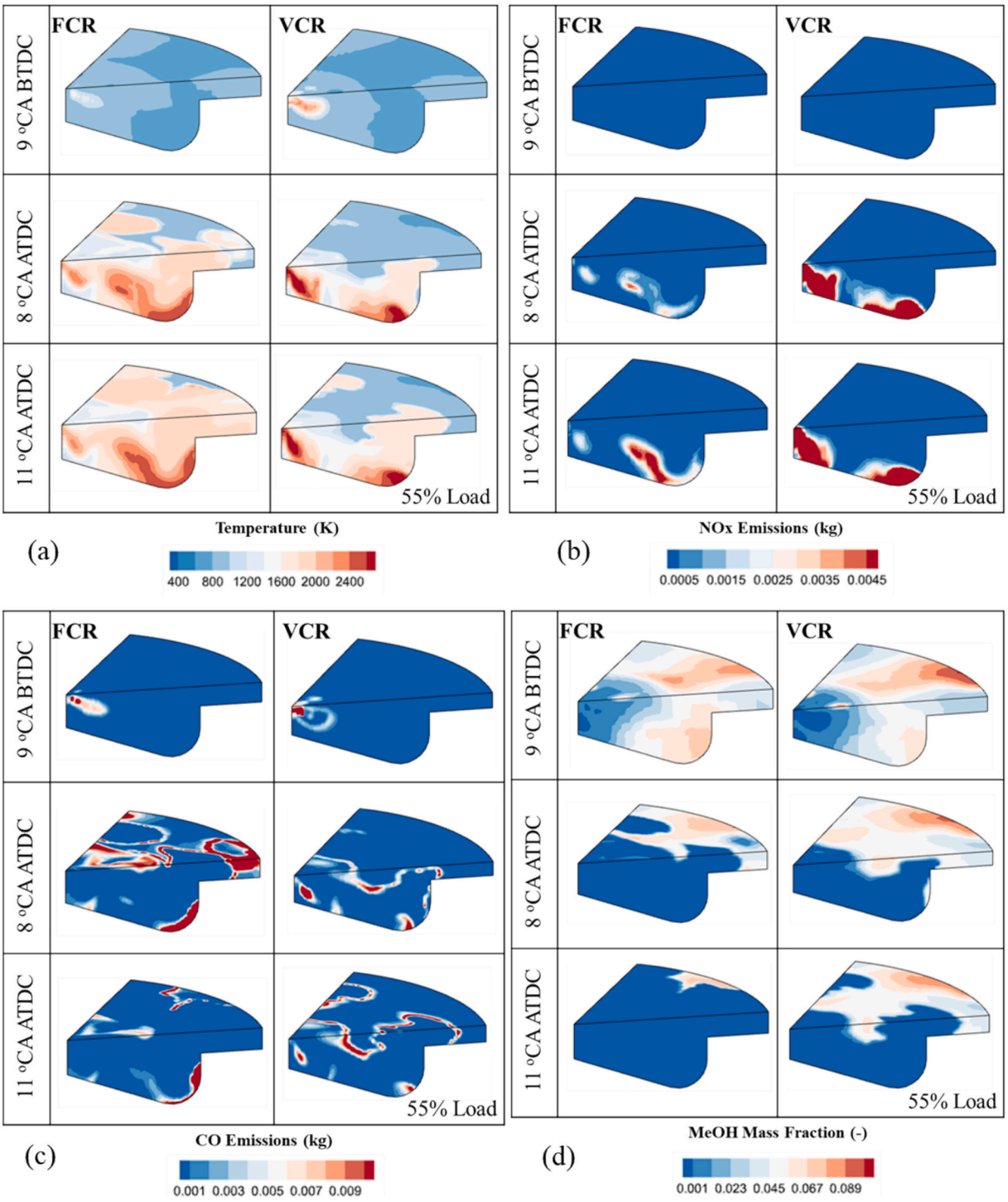

Fig. 6. Contours of (a) temperature, (b) NOx emissions, (c) CO emissions and (d) Methanol mass fraction spatial distribution in-cylinder for fixed and variable compression ratio engine types at 55 % load.

maximum in-cylinder pressure for the VCR cases is lower than in the FCR one (15.5 MPa for VCR and 17.1 MPa for FCR). This is attributed to the higher temperature at the inlet valve closing used for the FCR cases. The latter is deemed essential for achieving complete combustion conditions. VCR can achieve complete combustion conditions for lower charging temperature, exhibiting lower in-cylinder pressure and heat release rate peaks. However, combustion is prolonged, as CA90 is shifted from 10 ^{o}CA ATDC for the FCR to 25 ^{o}CA ATDC for VCR.

For the high load (90 %) operation, reduction of compression ratio leads to combustion kinetics inhibition, with expected reduction in reactivity. Therefore, combustion starts with burning of the high reactivity diesel close to TDC. Methanol combustion occurs gradually with reduced reaction kinetics from 5 ^{o}CA ATDC and CA90 is experienced at 20 ^{o}CA ATDC. FCR engine at high load yields maximum pressure close to 24 MPa due to the high MEF (90 %) utilised. Such elevated pressure is expected to drive the engine materials beyond their physical limits. The maximum in-cylinder temperature at the maximum cylinder pressure point reaches 2600 K in both FCR and VCR cases as presented in the in-cylinder contour of Fig. 3c. However, for VCR case, the combustion is shifted away from TDC, resulting in less time for the in-cylinder mixture

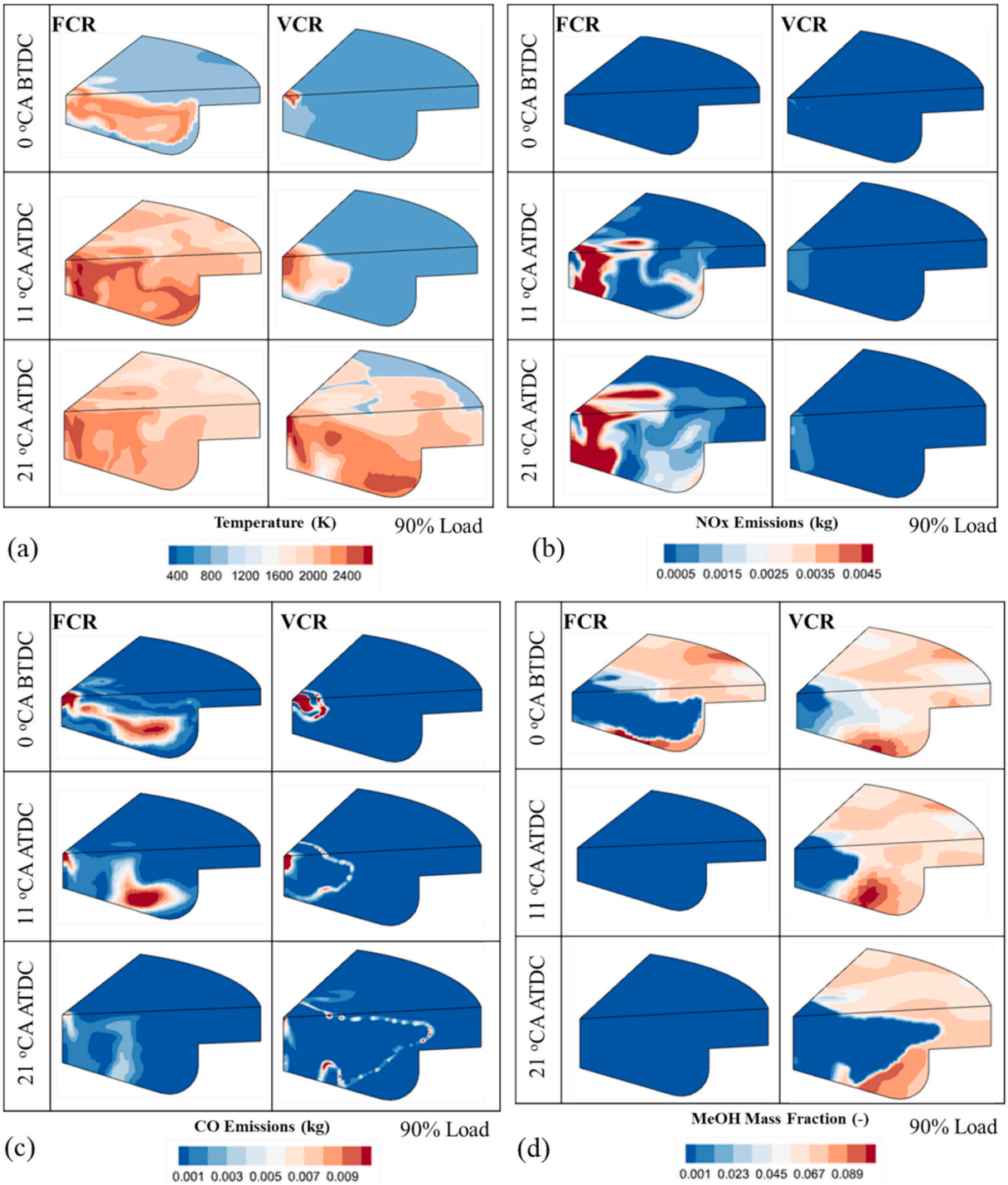

Fig. 7. Contours of (a) temperature, (b) NOx emissions, (c) CO emissions and (d) Methanol mass fraction spatial distribution in-cylinder for fixed and variable compression ratio engine types at 90 % load.

at temperatures above 1800 K yielding lower NOx emissions. With VCR engine type, such behaviour is mitigated as maximum pressure is close to 15 MPa as a result of compression ratio reduction. Further research on alternative injection strategies, and EGR techniques is expected to allow optimal in-cylinder pressure curve for VCR. Furthermore, the injection settings used herein are the ones optimised for the FCR [32]. VCR requires updated injection timings and injection strategy for improved efficiency. In 90 % load, high combustion efficiency is achieved despite prolonged injection duration and heterogenous mixtures. For FCR, the improved in-cylinder reactivity combined with methanol high laminar flame speed facilitates rapid and efficient combustion, even in stratified conditions. Similarly, for VCR with reduced in-cylinder reactivity due to lower CR of 12, pilot diesel injection ensures effective combustion.

The rate of pressure rise presented in Table 2, is 2.26, 0.99 and 2.48 MPa/^{o}CA for the three examined loads. The results indicate that the VCR engine is within acceptable limits (below the 10 MPa/^{o}CA threshold [49]) through the operating envelope.

Fig. 4 illustrates the brake specific NOx and hydrocarbon (HC) emissions. In the low load, NOx emissions only slightly vary (4.4 and 4.3 g/kWh for FCR and VCR, respectively). The increase of CR is counteracted by the reduced temperature at the inlet valve closing point. In the medium load, NOx emissions increase for VCR to 5 g/kWh compared to

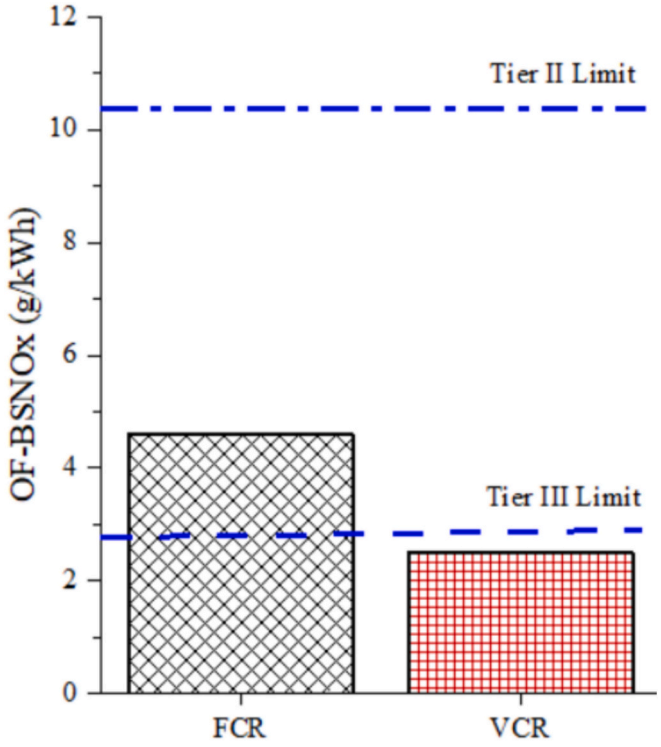

Fig. 8. Emission control areas, Tier III NOx compliance for the FCR (black line), VCR (red line) and VCR with EGR use (red-dashed line) engine types. (For interpretation of the references to colour in this figure legend, the reader is referred to the web version of this article.)

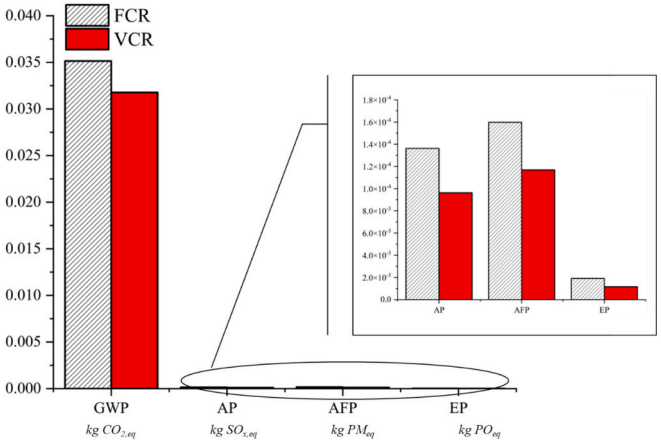

Fig. 9. Sustainability metrics for the engine with FCR and VCR settings.

1.6 g/kWh for FCR. This is due to compression ratio increase yielding higher in-cylinder temperature and pressure. Furthermore, for FCR, the use of 8 % EGR further suppresses NOx emissions. In the high load, due to combustion retardation, in-cylinder temperature is lower compared to FCR, yielding 69 % NOx emissions reduction for VCR.

For VCR, increasing CR at low load (20 %), yields complete combustion and hence the concentration of UM is reduced from 1.52 g/kWh to 0.21 g/kWh. At medium load (55 %), the charging temperature reduction for VCR, yields increased hydrocarbon emissions from 0.0007 g/kWh to 0.482 g/kWh. However, the effect on overall combustion efficiency is small as it reduces from 100 % for FCR to 99.87 % for VCR case. At high load, complete combustion is exhibited for both engine types. In all examined cases combustion efficiency remained above 99.8 %.

In order to capture the in-cylinder phenomena, the spatial distribution of temperature, NOx, CO emissions, and methanol mass fraction for the FCR and VCR cases at 20, 50 and 90 % load respectively. When in-cylinder temperature is discussed, the colour palette indicates the temperature variation from 400 K (blue) to 2400 K (red). Similarly, NOx emissions range from 0.002 kg (blue) to 0.018 kg (red) for low load, 0.0005 kg (blue) to 0.0045 kg (red) for medium load and 0.0005 kg (blue) to 0.0045 kg (red) for high load; CO emissions range from 0.001 kg (blue) to 0.009 kg (red) for all examined loads; methanol mass fraction 0.0002 (blue) to 0.0014 (red) for low load and 0.001 (blue) to 0.089 (red) form medium and high loads. The relevant colour scale is reported for each chart. For the low load operation (Fig. 5) the selected times refer to the FCR case capturing the 1st peak at the HRR curve (Fig. 3a) being at 10 ^{o}CA BTDC, the maximum HRR at 8 ^{o}CA ATDC and the CA90 point at 11 ^{o}CA BTDC. According to the analysis, flame propagation in both cases follows the same trend, and is concentrated in the bottom of the piston bowl. Since temperature exceeds the NOx cut-off one at 1800 K, NOx begin to form at 8 ^{o}CA ATDC at the flame front and close to the nozzle. CO emissions distribution indicate potential combustion inefficiency and comparing the two cases at the CA90 point, FCR presents greater CO concentration in-cylinder implying lower combustion efficiency than VCR. In both cases CO is concentrated on the top of the cylinder where temperature is lower and hence reactivity is inhibited. At the VCR case, the increased compression ratio offers the required reactivity due to higher pressure reached and therefore CO oxidation to CO_2.

For the medium load operation (Fig. 6) the selected times refer to the FCR case capturing the 1st peak at the HRR curve (Fig. 3b) being at 9 ^{o}CA BTDC, the maximum HRR at 8 ^{o}CA ATDC and the CA90 point at 11 ^{o}CA BTDC. The start of combustion is realised at 10 and 9 ^{o}CA BTDC for both VCR and FCR cases and hence small temperature differences are presented. As combustion propagates, higher compression ratio of the VCR case yields greater temperature in-cylinder and at 8 ^{o}CA ATDC the high temperature of the flame front (>2400 K) results in greater NOx concentration at the corners of the piston bowl. CO emissions are minimal in both cases as high reactivity in-cylinder yields complete combustion. Conversely, VCR case results in greatest unburned methanol implying prolonged combustion as opposed to FCR. At 11 ^{o}CA ATDC, at FCR case methanol is almost consumed with small parts being present close to the cylinder walls where heat transfer reduces the local temperature and inhibits combustion. For the VCR case, the lower rate of heat release prolongs combustion and methanol combusts slower. This justifies the increased overall NOx emissions benchmarked to FCR. Slow combustion increases the residency time of the in-cylinder mixture at elevated temperatures (>1800 K) hence favouring atmospheric nitrogen oxidation.

At high load operation (Fig. 7) the selected times refer to the VCR case capturing the 1st peak at the HRR curve (Fig. 3c) being at TDC, the maximum HRR at 11 ^{o}CA ATDC and the CA90 point at 21 ^{o}CA BTDC. Reducing the compression ratio for the VCR case results in significant ignition delay compared to FCR. Therefore, at the first peak of VCR heat release rate the combustion is close to the end for the FCR case. At 11 and 21 ^{o}CA ATDC combustion is at the expansion phase at FCR indicating that VCR case with reduced compression ratio require injection timings adjustment for optimal operation. Reduced cylinder reactivity offered by the reduction of CR in the VCR case, yields lower in-cylinder temperature and therefore NOx emissions reduce significantly. According to the CO contours, complete combustion is achieved in both cases. In both cases methanol injection has finished before the start of combustion and from the in-cylinder contour at TDC point, it is evident that it has occupied the cylinder volume. However, due to short time, the mixture is considered highly heterogenous penalising the indicated thermal efficiency and increases the susceptibility to unstable operation.

IMO Tier II and III NOx emission limits for the investigated engine correspond to 10.56 g/kWh and 2.65 g/kWh, respectively. Fig. 8 illustrates the NOx emissions as resulted from objective function described in

Eq.2. The engine with FCR settings complies with Tier II limits, however it does not achieve compliance with the Tier III limit. The engine with VCR settings achieves compliance with both Tier II and III limits with brake specific NOx emissions being 2.5 g/kWh, i.e., 7 % below the Tier III threshold.

Fig. 9 demonstrates the global warming, acidification, aerosol formation and eutrophication potentials, for the engine with FCR and VCR. The engine with VCR demonstrated 9.59 % greenhouse gas emissions reduction, which is mainly attributed to the lower N_2O emissions. Acidification potential reduces by 29.36 % due to improvement in NOx emissions for the engine with VCR. AFP improves by 26.86 % due to soot and NOx emissions reduction, whereas EP that is purely associated to NOx is reduced by 38.87 %. These results indicate an overall sustainability index improvement of 21 % for the engine with VCR compared to FCR.

3.1. Reflective discussion

This study investigated the potential of VCR in marine dual-fuel engines operating with 90 % methanol energy fraction to address key challenges, ensuring knock-free operation in high loads and misfiring-free operation in low loads. VCR facilitates the efficient combustion in the whole engine operating envelope without the need of EGR for achieving stable combustion conditions and reducing NOx emissions. By numerically demonstrating the potential of using high methanol energy fractions in marine engines, this study supports the transition to low-carbon fuels, aiding the shipping industry efforts to meet IMO 2050 GHG targets.

The study findings promote the adoption of methanol as a primary marine fuel, showcasing its viability and operational advantages in dual-fuel engines. This encourages diversification of fuel options in shipping, reducing dependence on traditional fossil fuels. Studies insights fill existing knowledge gaps regarding the integration of high methanol energy fractions in large-bore marine engines, providing valuable guidance for the engine efficiency improvement across diverse operating conditions. While the study focuses on marine four-stroke engines, the principles and benefits of VCR technology can be extended to other engine types, including rail and stationary power applications. Further research could refine the identified parameters, such as injection timing and dynamic adjustments, to explore the impact on methanol combustion stability.

4. Conclusions

This study investigated the use of variable compression ratio (VCR) settings in marine dual-fuel methanol fuelled engine considering different engine loads (20, 55 and 90 %). CFD models were developed for a marine four-stroke engine in different modes (diesel, gas, methanol dual-fuel) considering fixed and variable compression ratio (FCR and VCR) settings. A parametric optimisation study was contacted to select the CR settings for VCR. The derived performance and emissions parameters for the engine with FCR and VCR settings were compared, whereas compliance with the Tier III NOx limits was also discussed.

The main findings of this study are summarised as follows.

- The engine with VCR can effectively mitigate knocking at high loads and misfiring at low loads.
- The compression ratio reduction in the high load resulted in lower indicated thermal efficiency due to the decreased expansion ratio and lower NOx emissions due to the resultant in-cylinder reactivity decrease.
- VCR offers the flexibility to adjust compression ratio based on engine load exhibiting higher indicated thermal efficiency for a wider range of operating envelope compared to FCR.
- EGR use is not essential to achieve Tier III NOx compliance.
- The sustainability metrics indicate 9.59 %, 29.36 %, 26.86 % and 38.87 % reduction of GWP, AP, AFP and EP, respectively.
- Methanol dual-fuel marine engines with VCR exhibited sustainability index improved by 21 % compared to FCR.

The study demonstrated that the methanol-fuelled marine engines with VCR operating at 90 % methanol energy fraction yields stable operation and NOx emissions reduction, thus providing high decarbonisation potential of the shipping industry. Potential challenges are associated with the mechanical complexity and the cost effectiveness of the VCR systems. Future studies could focus on optimising the engine designs of VCR technologies for marine engines.

CRediT authorship contribution statement

Panagiotis Karvounis: Writing – review & editing, Writing – original draft, Software, Project administration, Methodology, Investigation, Conceptualization. **Gerasimos Theotokatos:** Writing – review & editing, Supervision, Project administration, Methodology, Investigation, Formal analysis, Data curation, Conceptualization.

Declaration of competing interest

The authors declare that they have no known competing financial interests or personal relationships that could have appeared to influence the work reported in this paper.

Acknowledgements

The authors greatly acknowledge the funding from DNV AS and RCCL for the MSRC establishment and operation. The opinions expressed herein are those of the authors and should not be construed to reflect the views of DNV AS and RCCL. CONVERGE was used for the CFD simulation. The opinions expressed herein are those of the authors and should not be construed to reflect the views of DNV AS, and RCCL.

Appendix A. Appendix

Table A1 lists the boundary and initial conditions used for the engine diesel mode.

Fig. A1 presents the NOx and Soot emissions validation for the dual-fuel operation of the light-duty engine. According to the results, NOx and Soot present errors below 7 % which falls within the computational model acceptance rate.

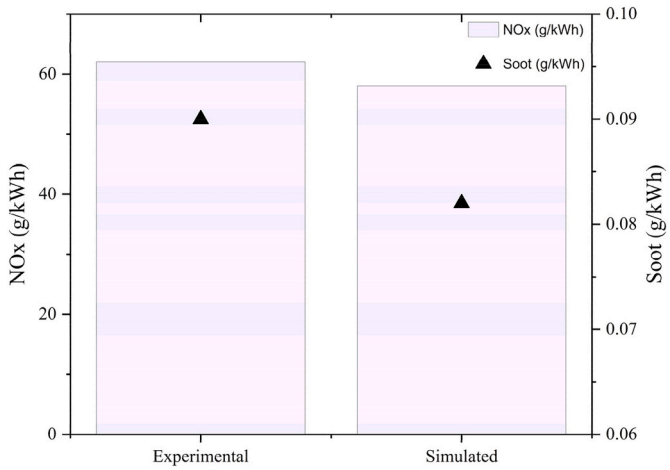

Fig. A1. NOx and Soot emissions for a high-speed light duty engine operating with 30 % methanol at 75 % load.

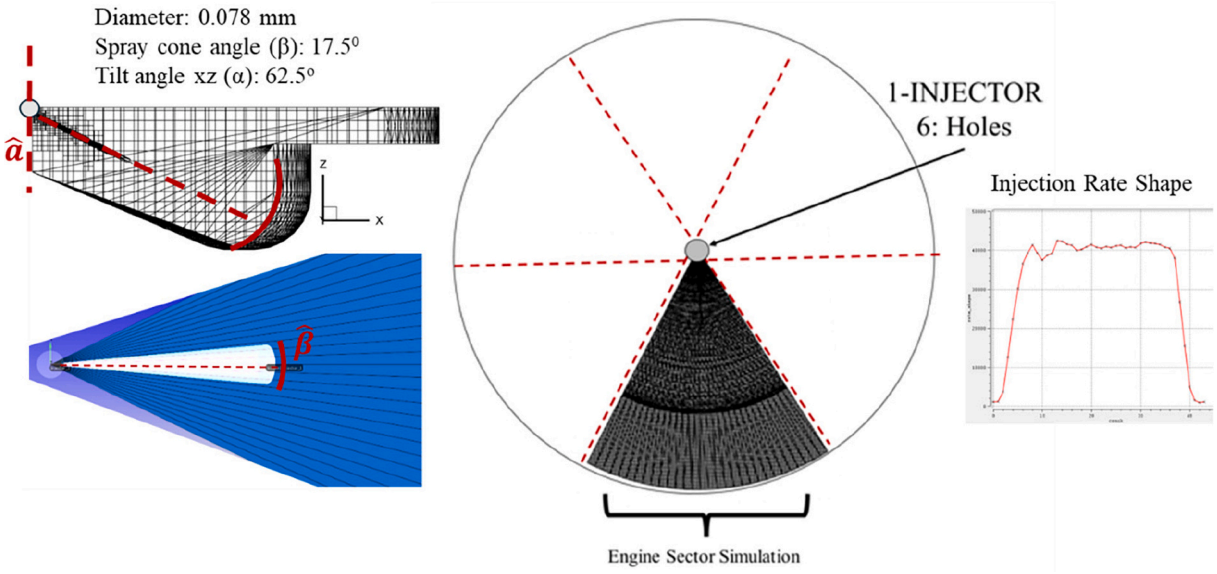

Fig. A2. Injector characteristics and computational domain.

Table A1
Boundary and initial conditions for the diesel operation model.

	Value	Explanation
Boundary conditions		
Cylinder head Temperature (K)	530	Calculated from the zero-dimensional thermodynamic model developed by Tsitsilonis et al. [26], pertaining to warmed up conditions of the engine.
Cylinder Wall Temperature (K)	430	
Piston Temperature (K)	550	
Initial conditions		
Temperature at the IVC (K)	360	Calculated the ideal gas law and the charging temperature and pressure from the shop trials.
Pressure at the IVC (bar)	2.8	
Turbulent kinetic energy (m^2/s^2)	62.02	Default values were used. A parametric study was conducted to determine their influence on the results.
Turbulent dissipation (m^2/s^3)	17,183	
Liquid diesel spray temperature at the time of injection (K)	340	Within the range of experimental results reported in Siebers [31].

Table A2 provides the grid characteristics employed in the grid sensitivity analysis.

Table A2
Computational grid data and derived results errors.

Parameter	Grid 1	Grid 2	Grid 3	Grid 4
Element size (mm)	12	10	8	6
Maximum Number of Cells*	10,900	18,838	36,800	87,216
Adaptive mesh refinement	On between 12 °CA BTDC and 135 °CA ATDC			
Velocity Max Embedding Level	3	3	4	4
Temperature Max Embedding Level	3	3	4	4
Number of Cores Used	40 Intel Cores IPM			
Simulation run duration (h)	3	4.5	9.5	23
Error on p_{max} (%)	5.2	2.4	2.3	2.3
RMSE on in-cylinder pressure (bar)	4.96	4.93	4.91	4.90

Table A3 lists the characteristics of the investigated marine engine and its injector.

Table A3
Includes the marine engine characteristics.

Parameter	Value
Type	Wärtsilä 9L46C
Combustion Method	Diffusive
Brake Power at MCR point (kW)	10,500
Speed at MCR point (r/min)	500
Cylinders Number (–)	9
Compression Ratio	14.0:1
Bore / Stroke (mm)	460 / 580
Nozzle angle (deg)	67.5
Spray Cone Angle (deg)	17.5
Nozzle Diameter (mm)	0.78
Nozzle Holes Number (–)	6
Simulated cycle period	IVC – EVO 135°CA BTDC–135°CA ATDC

For the sustainability analysis, the following metrics are calculated for the investigated engine considering VCR and FCR settings.

The Global Warming Potential (GWP) is calculated by the following equation considering the carbon dioxide (CO_2), methane (CH_4), and nitrous oxide (N_2O) emissions:

$$GWP = E_{CO_2} + 36\,E_{CH_4} + 298\,E_{N_2O}\left[kg_{CO_2eq}\right] \tag{A1}$$

The Acidification Potential (AP) refers to the emissions that cause acid rain. These include sulphur dioxide (SO_2) and nitrogen oxides (NOx). The acidification potential is usually characterised by the SO_2-equivalence and is calculated by:

$$AP = E_{SOx} + 0.7\,E_{NOx}\left[kg_{SOx\ eq}\right] \tag{A2}$$

The Aerosol Formation Potential (AFP) considers the PM, SOx, and NOx emissions relative to the 2.5 particulate matter equivalent and is calculated by using $PM_{2.5}$ equivalence factors for PM, SOx and NOx, respectively, according to the following equation:

$$AFP = 0.5\,E_{PM} + 0.54\,E_{SOx} + 0.88\,E_{NOx}\left[kg_{PMeq}\right] \tag{A3}$$

The Eutrophication Potential (EP) is defined as the potential to cause over-fertilisation of the water and soil resulting to growth of biomass and affecting costal ecosystems; it is calculated according to the following equation:

$$EP = 0.13\,E_{NOx}\left[kg_{POeq}\right] \tag{A4}$$

Although, GWP, AP, AFP and EP indexes are well established, their combination as Sustainability Index has not previously considered in literature. The weights are proposed based on the rationale provided in Table A4.

Table A4
Proposed weights for the sustainability index.

Index	Value	Rationale
GWP	0.5	The highest weight is assigned to GWP as reducing greenhouse gas (GHG) emissions is critical for achieving global climate change mitigation targets, particularly in the maritime sector's transition towards decarbonisation.
AP	0.2	Acidification potential, primarily caused by NOx and SOx emissions, affects ecosystems by contributing to acid rain, which is a significant environmental concern for marine operations.
AFP	0.1	Aerosol Formation Potential receives a lower weight as particulate matter emissions, are secondary concerns compared to GHG and acidification effects.
EP	0.2	Eutrophication potential is weighted equally with acidification because of its impact on aquatic ecosystems, particularly in coastal areas affected by nutrient runoff and NOx emissions.

Abbreviations

AFP	Aerosol Formation Potential
AP	Acidification Potential
ATDC	After Top Dead Centre
BTDC	Before Top Dead Centre
CA90	Crank Angle where 90 % of the fuel is combusted
CFD	Computational Fluid Dynamics
ECA	Emission Control Area
EGR	Exhaust Gas Recirculation
FCR	Fixed Compression Ratio
HC	Hydrocarbon
IMO	International Maritime Organisation
IVC	Inlet Valve Closing
LHV	Lower Heating Value
MEF	Methanol Energy Fraction
NOx	Nitrous Oxides
OF	Objective Function
RMSE	Root Mean Square Error
SI	Sustainability Index
SOI	Start of Injection
SOx	Sulphur Oxides
VCR	Variable Compression Ratio
VCR*	Variable Compression Ratio with EGR use

Nomenclature

CR	Compression Ratio

Data availability

No data was used for the research described in the article.

References

[1] E. Lindstad, P. Dražen, A. Rialland, I. Sandaas, T. Stokke, Reaching IMO 2050 GHG Targets Exclusively Through Energy Efficiency Measures, In SNAME Maritime Convention, 2022.

[2] P. Karvounis, C. Tsoumpris, E. Boulougouris, G. Theotokatos, Recent advances in sustainable and safe marine engine operation with alternative fuels, Front. Mech. Eng. (8) (2022 Nov 28) 994942.

[3] B. Ghorbani, M. Mehrpooya, F.K. Bahnamiri, An integrated structure of bio-methane/bio-methanol cogeneration composed of biogas upgrading process and alkaline electrolysis unit coupled with parabolic trough solar collectors system, Sustain. Energy Technol. Assess. (46) (2021 Aug 1) 101304.

[4] G. Theotokatos, P. Karvounis, G. Polychronidi, Environmental-economic analysis for decarbonising ferries fleets, Energies 16 (22) (2023 Nov 7) 7466.

[5] P. Karvounis, G. Theotokatos, I. Vlaskos, A. Hatziapostolou, Methanol combustion characteristics in compression ignition engines: a critical review, Energies 16 (24) (2023 Dec 14) 8069.

[6] Q. Huang, R. Yang, J. Liu, T. Xie, J. Liu, Investigation of the mechanism behind the surge in nitrogen dioxide emissions in engines transitioning from pure diesel operation to methanol/diesel dual-fuel operation, Fuel Process. Technol. (264) (2024 Nov 15) 108131.

[7] A. García, J. Monsalve-Serrano, C. Micó, M. Guzmán-Mendoza, Parametric evaluation of neat methanol combustion in a light-duty compression ignition engine, Fuel Process. Technol. (249) (2023 Oct 1) 107850.

[8] J. Dierickx, J. Verbiest, T. Janvier, J. Peeters, L. Sileghem, S. Verhelst, Retrofitting a high-speed marine engine to dual-fuel methanol-diesel operation: a comparison of multiple and single point methanol port injection, Fuel Commun. (7) (2021 Jun 1) 100010.

[9] Y Yang, W Long, P Dong, Y Qian, J Cao, D Dong, Performance of large-bore methanol/diesel dual direct injection engine applying asymmetrical diesel nozzle strategies, Applied Thermal Engineering 244 (2024, May 1) 122674.

[10] X. Yin, L. Xu, H. Duan, Y. Wang, X. Wang, K. Zeng, Y. Wang, In-depth comparison of methanol port and direct injection strategies in a methanol/diesel dual fuel engine, Fuel Process. Technol. (241) (2023 Mar 1) 107607.

[11] R.K. Maurya, A.K. Agarwal, Experimental investigations of performance, combustion and emission characteristics of ethanol and methanol fueled HCCI engine, Fuel Process. Technol. (126) (2014 Oct 1) 30–48.

[12] M.R. Saxena, R.K. Maurya, P. Mishra, Assessment of performance, combustion and emissions characteristics of methanol-diesel dual-fuel compression ignition engine: a review, J. Traffic Transp. Eng. (Engl. Ed.) 8 (5) (2021 Oct 1) 638–680.

[13] X. Yin, G. Yue, J. Liu, H. Duan, Q. Duan, H. Kou, Y. Wang, B. Yang, K. Zeng, Investigation into the operating range of a dual-direct injection engine fueled with methanol and diesel, Energy (267) (2023 Mar 15) 126625.

[14] H. Lu, A. Yao, C. Yao, C. Chen, B. Wang, An investigation on the characteristics of and influence factors for NO2 formation in diesel/methanol dual fuel engine, Fuel (235) (2019 Jan 1) 617–626.

[15] X. Yin, W. Li, H. Duan, Q. Duan, H. Kou, Y. Wang, B. Yang, K. Zeng, A comparative study on operating range and combustion characteristics of methanol/diesel dual direct injection engine with different methanol injection timings, Fuel (334) (2023 Feb 15) 126646.

[16] Q. Duan, X. Yin, X. Wang, H. Kou, K. Zeng, Experimental study of knock combustion and direct injection on knock suppression in a high compression ratio methanol engine, Fuel (311) (2022 Mar 1) 122505.

[17] L. Xu, M. Treacy, Y. Zhang, A. Aziz, M. Tuner, X.S. Bai, Comparison of efficiency and emission characteristics in a direct-injection compression ignition engine fuelled with iso-octane and methanol under low temperature combustion conditions, Appl. Energy (312) (2022 Apr 15) 118714.

[18] B. Gainey, J. Gandolfo, Z. Yan, B. Lawler, Mixing controlled compression ignition with methanol: an experimental study of injection and EGR strategy, Int. J. Engine Res. 24 (5) (2023 May) 1961–1972.

[19] M.D. Shields, J. Zhang, The generalization of Latin hypercube sampling, Reliab. Eng. Syst. Saf. (148) (2016 Apr 1) 96–108.

[20] L.M. Ricart, R.D. Reitz, J.E. Dec, Comparisons of diesel spray liquid penetration and vapor fuel distributions with in-cylinder optical measurements, J. Eng. Gas Turbines Power 122 (4) (2000) 588–595.

[21] N. Nordin, Complex Chemistry Modeling of Diesel Spray Combustion, PhD thesis, Chalmers University, 2001.

[22] Y.B. Zeldovich, The oxidation of nitrogen in combustion explosions, Acta Physicochim. U.S.S.R. 21 (1946) 577–628.

[23] X. Yin, W. Li, W. Zhang, X. Lv, B. Yang, Y. Wang, K. Zeng, Experimental analysis of the EGR rate and temperature impact on combustion and emissions characteristics in a heavy-duty NG engine, Fuel 310 (2022) 122394.

[24] J.C. Andrae, R.A. Head, HCCI experiments with gasoline surrogate fuels modeled by a semidetailed chemical kinetic model, Combust. Flame 156 (4) (2009 Apr 1) 842–851.

[25] M Wen, C Wang, Z Zhang, Y Wu, H Liu, C Jin, Z Zheng, M Yao, Effects of operating parameters on start performance of compression ignition engine by using high-pressure direct-injection pure methanol fuel, Appl. Therm. Eng. 249 (2024, Jul 15) 123352.

[26] KM Tsitsilonis, G Theotokatos, C Patil, A Coraddu, Health assessment framework of marine engines enabled by digital twins, International Journal of Engine Research 24 (7) (2023 Jul) 3264–3281.

[27] R. Wang, H. Chen, C. Guan, A Bayesian inference-based approach for performance prognostics towards uncertainty quantification and its applications on the marine diesel engine, ISA Trans. 118 (2021) 159–173, https://doi.org/10.1016/j.isatra.2021.02.024.

[28] RESOLUTION MEPC.177(58) Adopted on 10 October 2008 Amendments to the technical code on control of emissions of nitrogen oxides from marine diesel engines.
[29] J. Li, J. Wang, T. Liu, J. Dong, B. Liu, C. Wu, Y. Ye, H. Wang, H. Liu, An investigation of the influence of gas injection rate shape on high-pressure direct-injection natural gas marine engines, Energies 12 (13) (2019 Jul 4) 2571.
[30] C. Zhang, H. Wu, Combustion characteristics and performance of a methanol fueled homogenous charge compression ignition (HCCI) engine, J. Energy Inst. 89 (3) (2016 Aug 1) 346–353.
[31] D.L. Siebers, Liquid-phase fuel penetration in diesel sprays, SAE Trans. (1998 Jan 1) 1205–1227.
[32] P. Karvounis, G. Theotokatos, C. Patil, L. Xiang, Y. Ding, Parametric investigation of diesel–methanol dual fuel marine engines with port and direct injection, Fuel 381 (2025) 133441, https://doi.org/10.1016/j.fuel.2024.133441.
[33] R. Zang, C. Yao, Numerical study of combustion and emission characteristics of a diesel/methanol dual fuel (DMDF) engine, Energy Fuel 29 (6) (2015 Jun 18) 3963–3971.
[34] E. Randolph, R. Gukelberger, T. Alger, T. Briggs, C. Chadwell, A. Bosquez Jr., Methanol fuel testing on port fuel injected internal-only EGR, HPL-EGR and D-EGR® engine configurations, SAE Int. J. Fuels Lubr. 10 (3) (2017 Nov 1) 718–727.
[35] Y.D. Bharadwaz, B.G. Rao, V.D. Rao, C. Anusha, Improvement of biodiesel methanol blends performance in a variable compression ratio engine using response surface methodology, Alex. Eng. J. 55 (2) (2016 Jun 1) 1201–1209.
[36] P. Karvounis, G. Theotokatos, E. Boulougouris, Environmental-economic sustainability of hydrogen and ammonia fuels for short sea shipping operations, Int. J. Hydrog. Energy (57) (2024 Feb 29) 1070–1080.
[37] P. Karvounis, J.L. Dantas, C. Tsoumpris, G. Theotokatos, Ship power plant decarbonisation using hybrid systems and ammonia fuel—a techno-economic–environmental analysis, J. Mar. Sci. Eng. 10 (11) (2022 Nov 7) 1675.
[38] J.B. Heywood, Internal Combustion Engine Fundamentals, 2nd ed., McGraw-Hill Education, 2018.
[39] Z. Li, Y. Wang, Z. Yin, H. Geng, R. Zhu, X. Zhen, Effect of injection strategy on a diesel/methanol dual-fuel direct-injection engine, Appl. Therm. Eng. (189) (2021 May 5) 116691.
[40] Z. Li, Y. Wang, Y. Wang, Z. Yin, Z. Gao, Z. Ye, X. Zhen, Effects of fuel injection timings and methanol split ratio in M/D/M strategy on a diesel/methanol dual-fuel direct injection engine, Fuel (325) (2022 Oct 1) 124970.
[41] Y. Dong, O. Kaario, G. Hassan, O. Ranta, M. Larmi, B. Johansson, High-pressure direct injection of methanol and pilot diesel: a non-premixed dual-fuel engine concept, Fuel (277) (2020 Oct 1) 117932.
[42] M. Christensen, A. Hultqvist, B. Johansson, Demonstrating the multi fuel capability of a homogeneous charge compression ignition engine with variable compression ratio, SAE Trans. (1999 Jan 1) 2099–2113.
[43] D. Rabhi, V. Rabhi, P. Ranson, Gear design and dimensioning study for a variable compression ratio engine, SAE Tech. Pap. (2005, Jul 1). No. 2005-01-3131.
[44] S. Kojima, S. Kiga, K. Moteki, E. Takahashi, K. Matsuoka, Development of a new 2L gasoline VC-Turbo engine with the world's first variable compression ratio technology, SAE Tech. Pap. (2018 Apr 3). No. 2018-01-0371.
[45] C. Marten, D. Pendovski, S. Pischinger, W. Bick, A two-stage variable compression ratio system for large-bore engines with advanced hydraulic control circuit and mechanical locking device, SAE Int. J. Engines 15 (03-15-02-0011) (2021 Aug 19) 247–261.
[46] Dual fuel injector WO2016078735A1: https://patents.google.com/patent/WO2016078735A1/en.
[47] Pilot injection of dual fuel engines EP2562399A1: https://patents.google.com/patent/EP2562399A1/en.
[48] R.R. Renish, A.J. Selvam, R. Čep, M. Elangovan, Influence of varying compression ratio of a compression ignition engine fueled with B20 blends of sea mango biodiesel, Processes 10 (7) (2022 Jul 21) 1423.
[49] P. Karvounis, G. Theotokatos, Parametric optimisation of diesel–methanol injection timings of a dual-fuel marine engine operating with high methanol fraction using CFD, Appl. Therm. Eng. 264 (2025 Jan 4) 125433.
[50] C. Gong, D. Li, Z. Li, F. Liu, Numerical study on combustion and emission in a DISI methanol engine with hydrogen addition, Int. J. Hydrog. Energy 41 (1) (2016 Jan 5) 647–655.
[51] W. Sun, M. Jiang, L. Guo, H. Zhang, Z. Jia, Z. Qin, W. Zeng, S. Lin, G. Zhu, S. Ji, Y. Zhu, Numerical study of injection strategies for marine methanol/diesel direct dual fuel stratification engine, J. Clean. Prod. (421) (2023 Oct 1) 138505.
[52] J. Liu, Z. Liu, L. Wang, P. Wang, P. Sun, H. Ma, P. Wu, Numerical simulation and experimental investigation on pollutant emissions characteristics of PODE/methanol dual-fuel combustion, Fuel Process. Technol. (231) (2022 Jun 15) 107228.
[53] J.A. Badra, F. Khaled, M. Tang, Y. Pei, J. Kodavasal, P. Pal, O. Owoyele, C. Fuetterer, B. Mattia, F. Aamir, Engine combustion system optimization using computational fluid dynamics and machine learning: a methodological approach, J. Energy Resour. Technol. 143 (2) (2021 Feb 1) 022306.
[54] B. Fisher, C. Mueller, Effects of injection pressure, injection-rate shape, and heat release on liquid length, SAE Int. J. Engines 5 (2) (2012 May 1) 415–429.